Vertical cracks characterization using lock-in thermography: II. Finite cracks.

R. Celorrio[1], A.J. Omella[1], N.W. Pech-May[2,3], A. Oleaga[2], A. Mendioroz[2] and A. Salazar[2]

[1]Departamento de Matemática Aplicada, EINA/IUMA, Universidad de Zaragoza, Campus Río Ebro, Edificio Torres Quevedo, 50018 Zaragoza, Spain

[2]Departamento de Física Aplicada I, Escuela Técnica Superior de Ingeniería, Universidad del País Vasco UPV/EHU, Alameda Urquijo s/n, 48013 Bilbao, Spain

[3]Department of Applied Physics, CINVESTAV Unidad Mérida, carretera Antigua a Progreso km6, A.P. 73 Cordemex, Mérida Yucatán 97310, México

E-mail: **agustin.salazar@ehu.es**

Abstract

The aim of this work is to characterize vertical cracks of finite size and arbitrary shape using optically excited lock-in thermography. In the first place, we have solved the direct problem, which consists of calculating the surface temperature distribution when the shape, size and width of the vertical crack are known. To do this we have developed a new method based on discontinuous finite elements, which allows dealing even with very narrow cracks, for which classical finite element methods fail. The surface temperature of steel samples containing semi-infinite cracks and illuminated with a laser beam focused close to the crack has been measured using a lock-in thermography setup. A least square fit of the amplitude and phase of the surface temperature is used to retrieve the width and depth of the semi-infinite crack. A very good agreement between the nominal and retrieved values of both parameters is found, confirming the validity of the model.

Keywords: infrared thermography, crack detection, thermal waves, nondestructive evaluation.

PACS numbers: 66.70.+f 81.70.Fy 44.10.+I 66.30.Xj

1. Introduction

One of the main applications of active infrared thermography is the detection of small near-surface defects, as is the case of delaminations, corrosion, voids and cracks, in a nondestructive way [1,2]. In the last decade infrared thermography has demonstrated its ability to detect small cracks, both surface breaking and hidden beneath the surface. Vibrothermography has been successfully used to detect close cracks, i.e. cracks with lips in contact, in a wide variety of materials [3-8]. In this technique the sample is excited by an ultrasonic wave and the heat dissipated mechanically at the defect propagates to the surface indicating the presence of the defect on a cold background. However, vibrothermography can only detect the edges of open cracks since no rubbing takes place at the open surfaces [9]. For this kind of cracks optically stimulated thermography is the most appropriate technique, but the presence of the defect produces just a perturbation of the existing surface temperature field, generated by the external excitation.

Vertical cracks are especially elusive when using a homogeneous illumination, which produces a heat flux perpendicular to the sample surface. In this way, the crack hardly disperses the heat flux, resulting in a negligible change in the surface temperature. The detection this kind of cracks requires generating an asymmetric heat flux with respect to the crack position. In this way, the so-called flying spot method was introduced in the early nineties [10]. It is based on heating the sample with a moving laser spot or line and detecting the time evolution of the surface temperature with an infrared camera [11-17]. Using this method, cracks with openings as small as a few micrometers can be detected [14].

In the last years several approaches to characterize the geometrical parameters of the crack (depth, length, width, orientation…) have been published [18,19]. They take advantage of the asymmetry of the temperature field around the crack when focusing the laser beam at one side of the crack, since the crack acts as a thermal resistance, which partially blocks heat flux.

In Part I of this paper we focused on the characterization of infinite vertical cracks using lock-in thermography. This technique provides surface temperature amplitude and phase images with a very low noise level. For infinite vertical cracks we found an analytical expression for the surface temperature of a sample containing such a crack when the surface is illuminated by a modulated and focused laser spot close to the crack. The presence of the defect produces an abrupt jump in the amplitude and phase of the temperature profile at the crack position. This jump depends on four experimental parameters: laser beam radius, distance spot-crack, modulation frequency and width of the crack. The goal was to measure the thermal contact resistance R_{th} of the crack, which quantifies its width. Lock-in thermography measurements on stainless steel and vitreous carbon samples containing calibrated infinite cracks were performed. A least square fit of the surface temperature to the analytical model gave thermal resistances in very good agreement with the calibrated values for crack width down to 1 μm.

In this work, we have developed a new method to study the propagation of thermal waves across narrow vertical cracks of finite size and arbitrary shape in a homogeneous material. No analytical solution can be found for this problem so a numerical approach must be adopted. In classical continuous finite elements methods (FEM), this heat diffusion problem is modeled as a transmission problem in a material consisting of two domains, the bulk and the air filling the crack, together with the corresponding boundary conditions of continuity of temperature and heat flux [20]. In this model it is necessary to use conforming meshes, i. e. tetrahedral subdivisions of the domains, in both the exterior and the interior of the crack, matching at the interfaces. Therefore, for very thin cracks this model requires excessively fine meshes, dramatically increasing memory resources and computing time. To

overcome this problem, we have developed new numerical methods much more efficient than continuous FEM, which allow us to calculate the surface temperature of a sample containing thin cracks of any size and shape. These thin cracks are considered as an interface characterized by its thermal contact resistance R_{th}. The new methods are based on Discontinuous Galerkin finite elements methods (DG-FEM) [21]. In general, DG-FEM are natural tools to tackle physical problems with discontinuous solutions where classical FEM fail. However, the implementation of DG-FEM is not as straightforward as when dealing with continuous FEM, since DG-FEM require stabilization terms, depending on each particular problem. In Section II, we expand the Bauman-Oden DG-FEM for the Laplace equation [21], in order to model the propagation of thermal waves in cracked materials.

2. Theory

In this section, we present new numerical DG methods, providing the essential information needed for direct implementation in software packages of finite elements. We consider a cracked opaque sample occupying volume Ω, limited by a surface boundary $\partial\Omega$. The geometry is depicted in Fig. 1a. The sample contains a narrow crack extending along Γ_C. Since the crack is very thin, we assume that Γ_C is an interface. Part of the sample surface Γ_g is illuminated by a laser beam modulated at frequency *f*. The non-illuminated section of the boundary is denoted as Γ_0. The oscillating component of the sample temperature $T(r)$ can be obtained by solving the Helmholtz equation with the appropriate boundary and transmission conditions of temperature and heat flux:

$$\Delta T(\vec{r}) + \frac{i2\pi f}{D} T(r) = 0, \qquad r \in \Omega \setminus \Gamma_C \tag{1a}$$

$$\left(K \frac{\partial T_-}{\partial n_-} + K \frac{\partial T_+}{\partial n_+} \right)\Bigg|_{\Gamma_C} (\vec{r}) = 0, \qquad r \in \Gamma_C \tag{1b}$$

$$(T_- - T_+)\big|_{\Gamma_C} (\vec{r}) + R_{th}(r) K \frac{\partial T_-}{\partial n_-}\Bigg|_{\Gamma_C} (r) = 0, \qquad r \in \Gamma_C \tag{1c}$$

$$\frac{\partial T}{\partial n}\Bigg|_{\Gamma_0} (\vec{r}) = 0, \qquad r \in \Gamma_0 \tag{1d}$$

$$K \frac{\partial T}{\partial n}\Bigg|_{\Gamma_g} (\vec{r}) = g(r), \qquad r \in \Gamma_g \tag{1e}$$

where K and D are the thermal conductivity and diffusivity of the sample respectively, subscripts + and – refer to both sides of the crack (no matter which is which), $\hat{n}$ is the outward unitary normal vector at the sample surface, $\hat{n}_+$ and $\hat{n}_-$ are the outwards unitary normal vectors at the crack sides, and $g(r)$ is the ingoing heat flux applied on the illuminated part of the sample boundary.

The first step to apply a DG method to solve Eq. (1) is to define a "triangulation" $\{K_j\}_{j=1}^{M}$ of the total volume, being K_j each of the M tetrahedra (see Fig. 1b). The faces of the tetrahedra kissing the crack must match the crack surface. The second step is to choose simple piecewise functions T_h (for instance polynomials of degree m) to approximate the temperature T in each tetrahedron. For practical purposes, the final step is to write a discrete variational formulation from Eq. (1) by using Green's formula and defining the so-called *numerical fluxes* [21], i.e. approximations to T and ∇T on the boundaries of each tetrahedron. The

fluxes choices affect the stability and the accuracy of the method and, therefore, different choices lead to different methods.

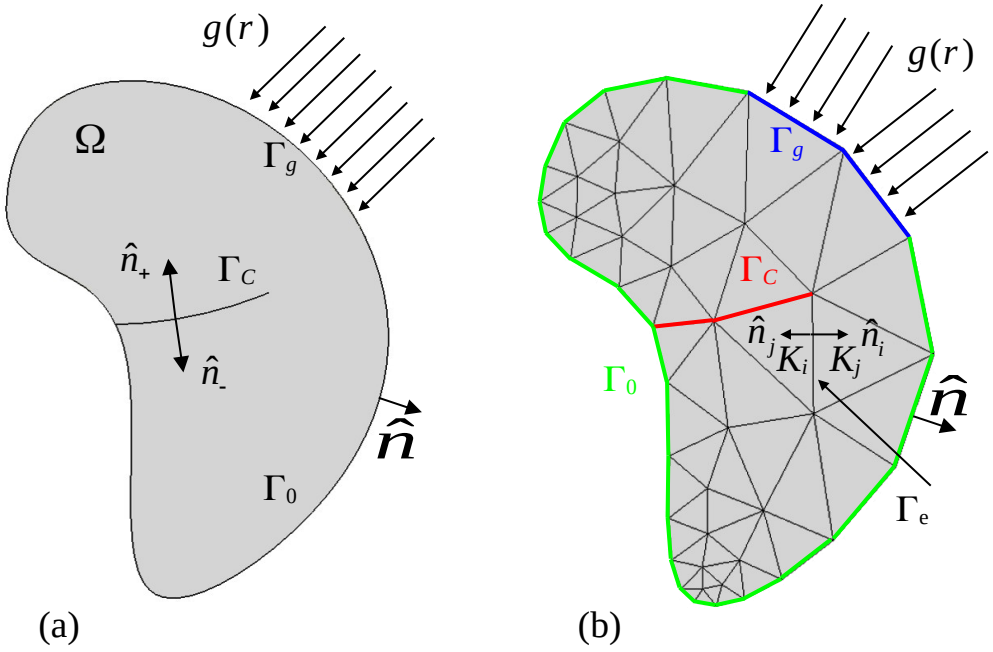

Figure 1. (a) Diagram of an opaque material of arbitrary shape containing a finite crack. Γ_g is the illuminated surface, Γ_C is the crack surface, Γ_0 is the non-illuminated external surface of the material, and Ω is the sample volume. (b) Diagram of the meshed sample showing tetrahedra comforming with the crack.

Any variational formulation of a DG method necessitates the introduction of the so-called *averages* and *jumps* traces of functions defined on the triangulation [21]. Let $\Gamma = \left(\cup_{j=1}^{M} \partial K_j\right) \setminus \left(\Gamma_c \cup \partial\Omega\right)$ be the *skeleton* of the triangulation, that is, all faces of the tetrahedra that belong neither to the crack nor to the exterior boundary. Let Γ_e be an interior face shared by two tetrahedra K_i and K_j, and w any scalar or vector function on Ω, we set the *averages* $\langle w \rangle$ and *jumps* $[\![w]\!]$ on Γ_e as:

$$\langle w \rangle = \frac{1}{2}\left(w_i + w_j\right), \tag{2a}$$

$$[\![w]\!] = w_i \cdot \hat{n}_i + w_j \cdot \hat{n}_j, \tag{2b}$$

being $\hat{n}_i$ and $\hat{n}_j$ the outwards unitary normal vectors to K_i and K_j respectively, as can be seen in Fig. 1b.

Thus, applying Green's formula [20] in a standard way in each tetrahedron the DG solution of Eqs. (1) is the m-degree polynomial piecewise function $T_h \approx T$ that satisfies the variational formulation

$$\sum_{j=1}^{M} \int_{K_j} \nabla T_h \nabla v_h - \int \langle \nabla T_h \rangle [\![v_h]\!] + \int_{\Gamma_C} \frac{1}{R_{th}(\vec{r}) K} [\![T_h]\!] [\![v_h]\!] - \frac{i2\pi f}{D} \int_{\Omega} T_h v_h = \frac{1}{K} \int_{\Gamma_g} g(\vec{r}) v_h, \tag{3}$$

for all *m*-degree polynomial piecewise functions v_h in the triangulation $\left\{ K_j \right\}_{j=1}^{M}$ of Ω.

Unluckily the variational formulation in Eq. (3) is unstable (it amplifies rounding errors) but fortunately it is possible to stabilize it by adding perturbation terms, related to particular choices of the numerical fluxes, that actually are null for the exact solution (but not for the approximate solution) and do not damage the numerical solution at all. A proper DG variational formulation of Eq. (1), based on the Bauman-Oden choice [21] of the numerical fluxes, is:

$$\sum_{j=1}^{M} \int_{K_j} \nabla T_h \nabla v_h - \int_{\Gamma} \langle \nabla T_h \rangle [\![v_h]\!] + \int_{\Gamma} [\![T_h]\!] \langle \nabla v_h \rangle + \int_{\Gamma_C} \frac{1}{R_{th}(r) K} [\![T_h]\!] [\![v_h]\!] - \frac{i2\pi f}{D} \int_{\Omega} T_h v_h = \frac{1}{K} \int_{\Gamma_g} g(\vec{r}) v_h \tag{4}$$

The third addendum in Eq. (4) is an antisymmetric version of the second one and comes from the Bauman-Oden choice of the numerical fluxes. It is introduced in order to stabilize the numerical results of Eq. (3).

From a practical point of view, the variational formulation is a cornerstone to introduce the DG model in finite elements packages as FEniCS or FreeFem++ [22,23]. The Bauman-Oden-type formulation shown in Eq. (4) is useful to simulate thermal waves in cracked materials when the location of the crack Γ_C is well known. However, due to the presence of the thermal resistance in the denominator, Eq. (4) suffers from a computational limitation: the narrower the crack, the greater the computing time required in simulations. Furthermore it is not possible to plug a zero thermal resistance in the fourth addendum of Eq. (4). This is a hard impediment when solving inverse problems, in which we attempt to determine the thermal resistance from surface thermograms by a least squares fitting, without previous knowledge of the (eventually null) value of the thermal resistance in the trial location Γ_C. Therefore, it is necessary to develop variational formulations whose computational time is independent of the value of the thermal resistance, and that admit zero thermal resistances in a trial location Γ_C probably larger than the real crack.

Let be $h_e = \frac{1}{2}\left(h_{K_i} + h_{K_j} \right)$ the average linear size of two tetrahedra K_i and K_j that share face Γ_e; that is, the average size of the diameters of the smallest circumscribed sphere around each tetrahedron. The variational formulation of the new DG method we propose is:

$$\begin{aligned} &\sum_{j=1}^{M} \int_{K_j} \nabla T_h \nabla v_h - \frac{i2\pi f}{D} \int_{\Omega} T_h v_h - \int_{\Gamma} \langle \nabla T_h \rangle [\![v_h]\!] + \int_{\Gamma} [\![T_h]\!] \langle \nabla v_h \rangle \\ &\quad - \int_{\Gamma_C} \frac{h_e}{h_e + C R_{th}^2(r) K} \langle \nabla T_h \rangle [\![v_h]\!] + \int_{\Gamma_C} \frac{h_e}{h_e + C R_{th}^2(r) K} [\![T_h]\!] \langle \nabla v_h \rangle \\ &\quad + \int_{\Gamma_C} \frac{h_e R_{th}(r) K}{h_e + C R_{th}^2(r) K} \langle (\nabla T_h \cdot \hat{n}) \hat{n} \rangle \cdot \langle (\nabla v_h \cdot \hat{n}) \hat{n} \rangle + \int_{\Gamma_C} \frac{C R_{th}(r)}{h_e + C R_{th}^2(r) K} [\![T_h]\!] [\![v_h]\!] = \frac{1}{K} \int_{\Gamma_g} g(\vec{r}) v_h \end{aligned} \tag{5}$$

being $\hat{n}$ the unitary outwards normal vectors to the tetrahedral. In fact, Eq. (5) represents a family of DG methods depending on the value of constant *C*. We have analyzed the methods corresponding to $C = 0$, $C = 1$ W/(m^{2}K) and $C = 1/R_{th}$. The three methods are robust and computationally efficient. However, for the sake of simplicity and rapidness we have chosen $C = 0$ for the numerical computations in this paper. Notice that for $C = 0$ and $C = 1$ W/(m^{2}K) Eq. (5) reduces to the classical Bauman-Oden method [21] for non-cracked materials when R_{th} is null. The computation time of these three methods is independent of the value of the thermal resistance.

Finally, let us remark that both Eqs. (4) and (5) require *m*-degree polynomial piecewise function $T_h \approx T$ with degree $m \geq 2$. This is a purely mathematical requirement for

the stability of DG Bauman-Oden-type methods and it has to be taken into account just in the selection of the trial functions in finite element packages as FEniCS or FreeFem++ [22,23].

3. Numerical simulations

Figure 2a shows the geometry of a vertical crack of arbitrary shape and size. Although the theoretical model developed in the previous section is valid for vertical cracks of any shape and size, we mainly performed numerical simulations for surface breaking semi-infinite cracks (infinite lateral extension and constant depth b), since preparing samples with calibrated cracks of this shape is easier. The geometry of these cracks is given in Fig. 2b and their discretization is shown in Fig. 3. As can be seen, the centered and densely discretized area corresponds to the iluminated zone around the center of the laser spot. In order to capture the geometrical characteristic lengths and the natural thermal wavelength $2\pi\mu$ of the solution, the size of the tetrahedra is between min(b/2, a/4, μ/3) and 2μ, where $\mu = \sqrt{D/(\pi f)}$ is the thermal diffusion length.

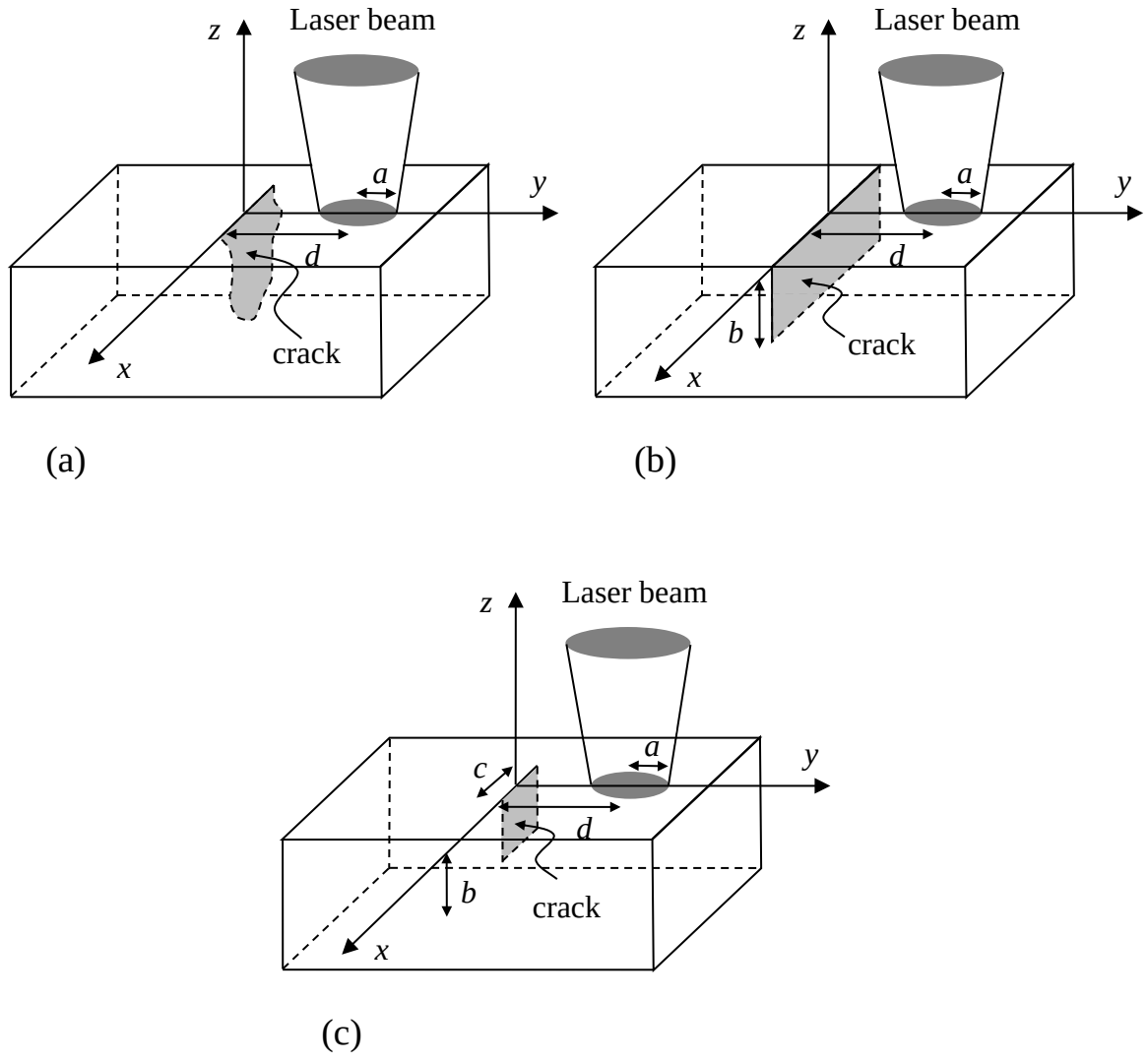

Figure 2. Scheme of (a) a finite vertical crack (in gray) of arbitrary shape, (b) a semi-infinite vertical crack (in gray) of height b and (c) a rectangular vertical crack (in gray) of height b and length c.

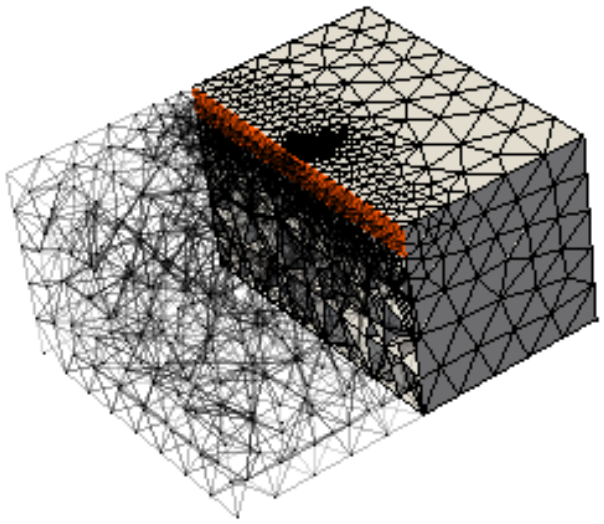

Figure 3. Mesh with 6,491 tetrahedra of a cracked thermally thick prism of AISI-304 with dimensions 10μ × 8μ × 5μ for a modulation frequency f = 0.6 Hz. A semi-infinite crack with depth b = 1 mm is depicted in red.

In Part I of this paper, when working with infinite cracks, we found that the highest temperature contrast at the crack position is produced when $d \approx \mu \approx 1.25a$. In this work, we keep these conditions and analyze the influence of the crack depth b on the temperature profile across the crack. Simulations are performed for AISI-304 stainless steel (D = 4.0 mm^2/s and K = 15 Wm^{-1}K^{-1}). As a first test of consistency we have calculated the temperature profile corresponding to an infinite crack ($b = \infty$) both using the analytical solution given by Eq. (10) in Part I of this paper and using the numerical solution as expressed by Eq. (5) in the previous section. The agreement is excellent for all the thermal resistances checked, ranging from 10^{-7} - 10^{-1} m^{2}K/W.

Figure 4 shows the natural logarithm of the temperature amplitude Ln|T| and phase Ψ along the y axis for an AISI-304 sample containing a semi-infinite vertical crack (y = 0) and illuminated by a circular Gaussian spot. Calculations are performed using Eq. (5) with d = 1 mm, a = 0.75 mm, f = 1 Hz and R_{th} = 10^{-3} m^{2}K/W (which is equivalent to a crack thickness of 25 μm). Four crack depths are analyzed b = 0.25, 0.5, 1 and 2 mm besides the infinite one. As can be seen, as the crack depth diminishes the height of the jump of Ln|T| at the crack position (y = 0) is reduced. The phase behavior is more complicated, but being its jump systematically much smaller than the jump in Ln|T| (the same scale level is used for both) it becomes less useful to obtain information on the crack depth.

To quantify the temperature jump at the crack position we introduce the temperature amplitude $\Delta_{|T|}$ and phase Δ_{Ψ} contrasts, which are defined respectively as

$$\Delta_{|T|} = \frac{|T(0,\varepsilon,0)| - |T(0,-\varepsilon,0)|}{|T(0,d,0)|}, \qquad (6)$$

$$\Delta_{\Psi} = \Psi(0,\varepsilon,0) - \Psi(0,-\varepsilon,0), \qquad (7)$$

where ε represents an infinitesimal distance.

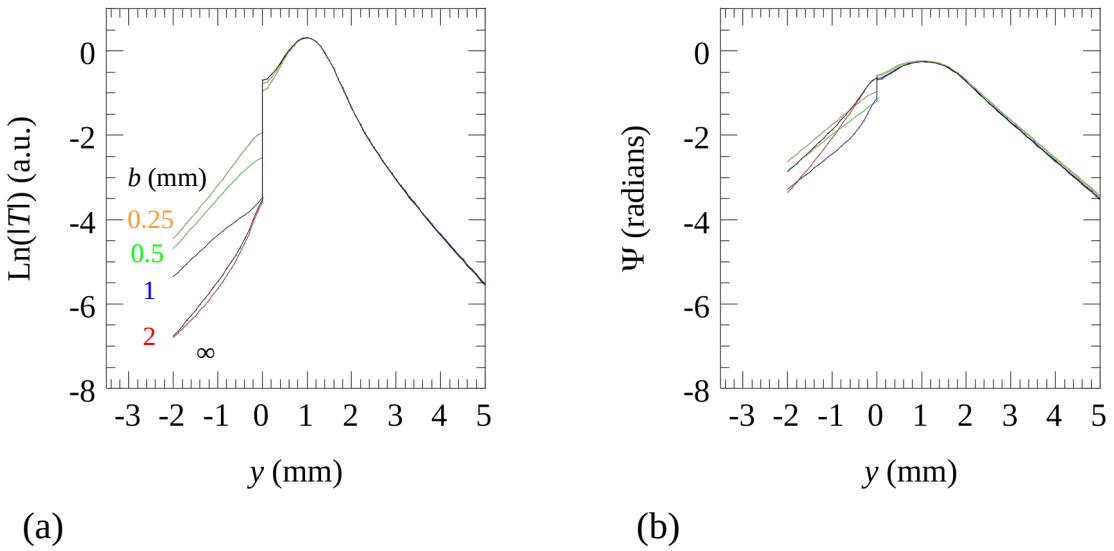

(a) (b)

Figure 4. Simulation of (a) the natural logarithm of the temperature amplitude and (b) phase along the y axis for an AISI-304 sample (D = 4 mm^2/s and K = 15 Wm^{-1}K^{-1}) containing a semi-infinite vertical crack of R_{th} = 10^{-3} m^{2}K/W. The sample is illuminated at d = 1 mm with a Gaussian laser spot of a = 0.75 mm modulated at f = 1 Hz. Several crack depths b are studied.

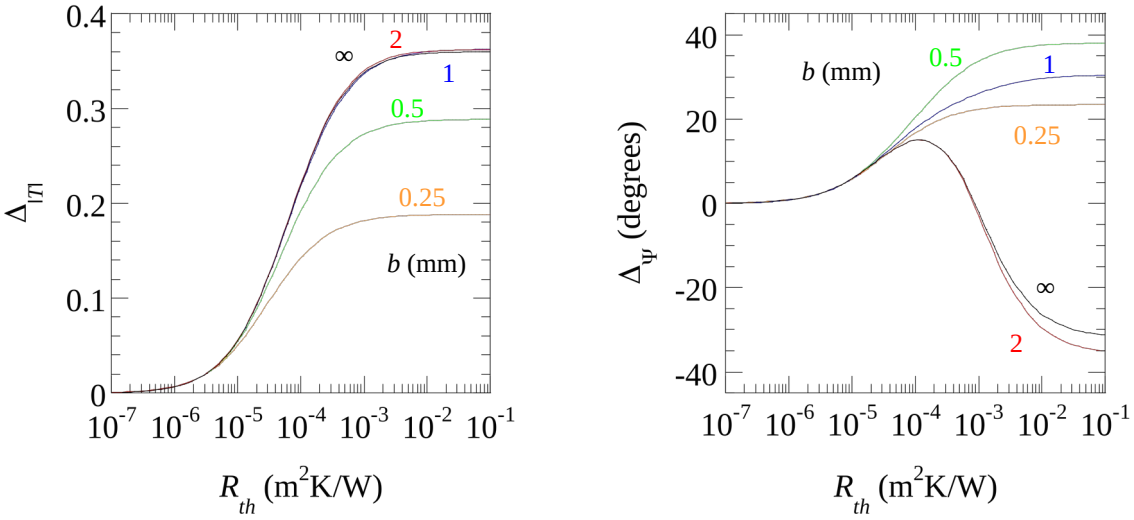

(a) (b)

Figure 5. Numerical simulation of the dependence of $\Delta_{|T|}$ and Δ_{Ψ} on the thermal contact resistance R_{th}. Calculations are performed for an AISI-304 sample (D = 4 mm^2/s and K = 15 Wm^{-1}K^{-1}) with d = 1 mm, a = 0.75 mm and f = 1 Hz. Several crack depths b are analyzed.

In Fig. 5 we analyze the dependence of $\Delta_{|T|}$ and Δ_{Ψ} on the thermal resistance of the crack for different crack depths. Calculations are performed with the same parameters as in Fig. 2 (d = 1 mm, a = 0.75 mm, f = 1 Hz). For R_{th} < 10^{-6} m^{2}K/W (crack width narrower than 25 nm) the temperature contrast is negligible and the crack remains undetected. As R_{th}

increases, $\Delta_{|T|}$ is enhanced until it reaches an asymptotic value. This value highly depends on the crack depth. For instance, the maximum value of $\Delta_{|T|}$ for b = 0.25 mm is half of the value reached for an infinite crack. However, the behavior of Δ_{Ψ} is not monotonous. It changes from negative values for deep crack to positive values for shallow cracks. Anyway, results shown in Figs. 4 and 5 (where the modulation frequency is kept constant f = 1 Hz) indicate that cracks deeper than 1.5 mm are difficult to distinguish from infinite cracks.

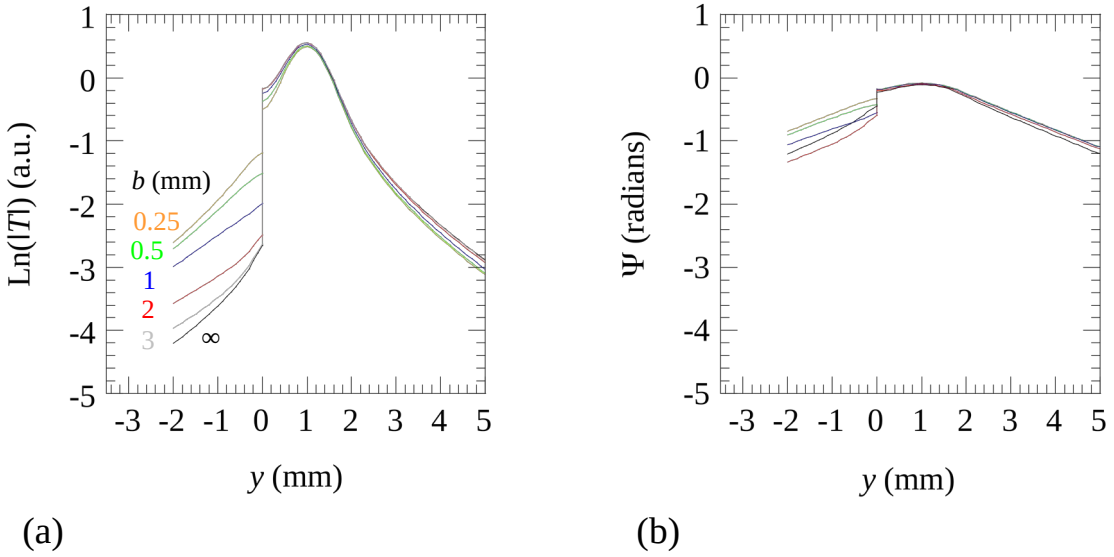

Figure 6. The same as in Fig. 4 for f = 0.1 Hz.

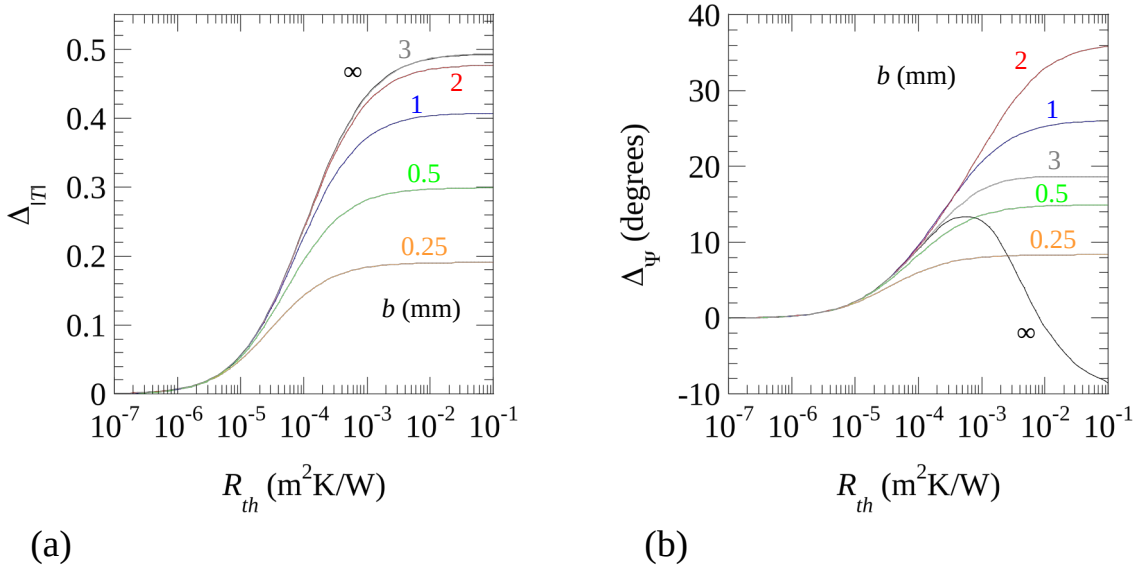

Figure 7. The same as in Fig. 5 for f = 0.1 Hz.

To enhance this limit we tried using lower frequencies which means launching thermal waves of larger wavelength. Figure 6 shows the simulation of the same Ln|T| and Ψ profiles along the y axis as in Fig. 4, but reducing the modulation frequency from 1 Hz to 0.1 Hz.

Additionally, Fig. 7 shows the same dependence of $\Delta_{|T|}$ and Δ_{Ψ} on the thermal resistance of the crack as in Fig. 5, but for a modulation frequency f = 0.1 Hz. As it is expected, by reducing the frequency we can look deeper inside the sample, in such a way that cracks as deep as 3.5 mm can be distinguished from an infinite one. Note that the limiting distinguishable depth verifies the following relation: $b_{limit} \approx \mu$.

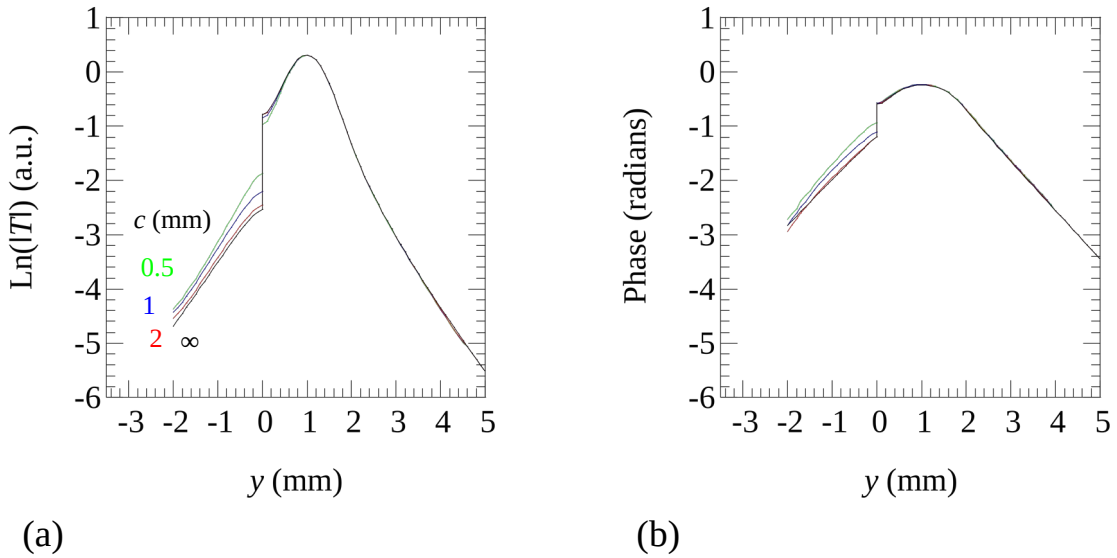

Figure 8. Simulation of (a) the natural logarithm of the temperature amplitude and (b) phase along the y axis for an AISI-304 sample containing a rectangular vertical crack of R_{th} = 10^{-3} m^{2}K/W. The sample is illuminated at d = 1 mm with a Gaussian laser spot of a = 0.75 mm modulated at f = 1 Hz. The depth b = 0.5 mm is kept while several lengths c are studied.

Finally, in order to show the usefulness of the discontinuous finite elements to deal with vertical cracks of any shape, we performed simulations for rectangular cracks of depth b and length c, centered on the y axis (see Fig. 2c). In Fig. 8 we show the simulation of Ln(|T|) and Ψ along the y axis for an AISI-304 sample containing a rectangular vertical crack. The same parameters as in Fig. 4 are used (R_{th} = 10^{-3} m^{2}K/W, d = 1 mm, a = 0.75 mm and f = 1 Hz). The crack depth b = 0.5 mm is kept fixed while the effect of changing its length c is studied. As can be observed, as the crack length decreases the height of the jump of Ln|T| and Ψ at the crack position (y = 0) is reduced. It is worth noting how such a small crack with an area 0.5 × 0.5 mm^2 is clearly detected by a high enough jump. Anyway, for retrieving the two parameters characterizing a rectangular crack (b and c) with the highest accuracy we can fit several temperature profiles (not just x = 0) and several frequencies for each of them.

It is worth noting that all the numerical simulations of this section use polynomial functions of degree 2 and have been performed with an Intel Pentium(R) 4 CPU 3.0 GHz × 2 with a RAM of 1.5 GiB. The computing time of a simulation is about 2 minutes.

4. Experimental results

The scheme of the lock-in thermography setup was described in Fig. 8 of Part I of this paper. In order to prepare calibrated semi-infinite vertical cracks, a thin film of thickness L was inserted between two blocks and buried at a depth b beneath the surface (see Fig. 9). Blocks and film are made of AISI-304 stainless steel. Some pressure was applied at the outer edges of the blocks to keep the best thermal contact between them and the film. We picked

two films thicknesses, namely L = 25 and 12.5 μm. Taking into account the relationship between the air gap of the crack and its thermal resistance $R_{th} = L / K_{air}$ [24], they represent thermal resistances of 10^{-3} and 5×10^{-4} m^{2}K/W respectively. Two depths were selected: b = 0.7 and 1.1 mm. As the steel blocks have shiny surfaces, a thin graphite layer about 3 μm thick was deposited onto the surface in order to increase both the absorption of the heating laser and the emissivity at infrared wavelengths.

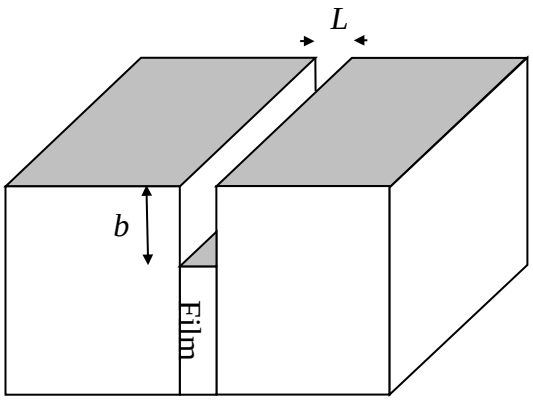

Figure 9. Diagram of the semi-infinite vertical crack simulated for the experiment: A thin film of thickness L is sandwiched between two blocks and is buried at a depth b beneath the surface. Blocks and film are made of the same material AISI-304 stainless steel.

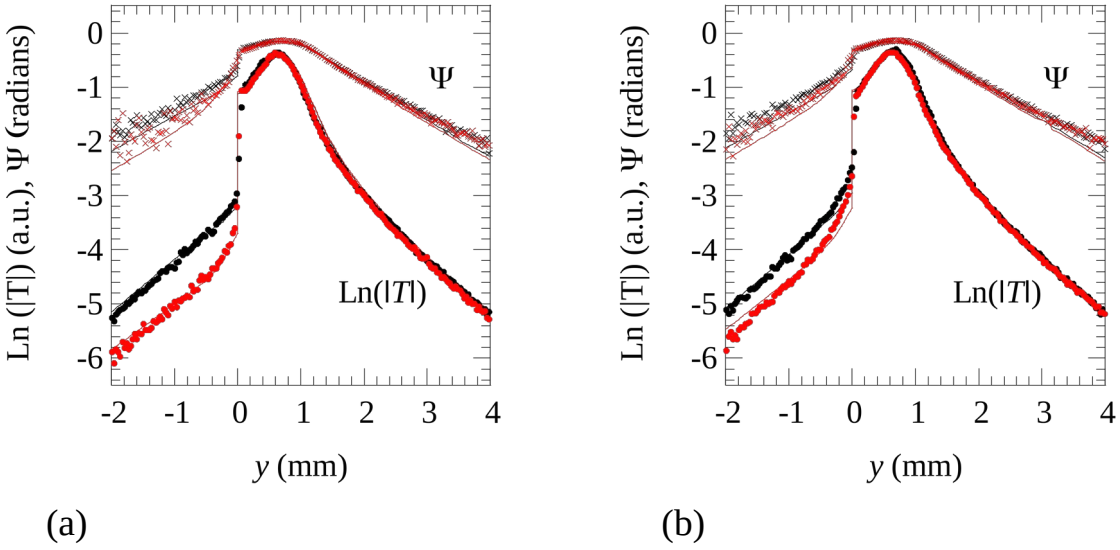

Figure 10. Experimental Ln(|T|) and Ψ of the surface temperature along the y axis for two AISI-304 stainless steel blocks sandwiching a thin film (a) 25 μm and (b) 12.5 μm thick of the same material. The thin film is buried at two different depths b = 0.7 mm (black) and 1.1 mm (red). Measurements have been performed with f = 0.6 Hz, d ≈ 0.65 mm and a ≈ 0.50 mm. Symbols correspond to experimental data and continuous lines to the fit to Eq. (5).

First, we have evaluated the additional thermal resistance due to the lack of perfect thermal contact between film and blocks. To do this we put the film just reaching the surface, i.e. b = 0. In this way, we have two infinite vertical cracks of approximately the same width, that according to the in-series thermal resistor model [25] are equivalent to a unique crack

with double thermal resistance. We measured the temperature profiles (amplitude and phase) along the *y* axis using the following experimental parameters f = 0.6 Hz, $d \approx$ 0.65 mm and $a \approx$ 0.50 mm. By fitting this temperature profile either to Eq. (10) in Part I of this paper or to Eq. (5) in section II we obtained a thermal resistance $R_{th} \approx 1\times10^{-5}$m^{2}K/W, which is equivalent to an air gap $L \approx$ 0.25 μm. Such a small value can be neglected if compared to air gaps of the simulated crack (12.5 - 25 μm). Accordingly, we assume a perfect thermal contact between film and steel blocks.

In Fig. 10a we show by symbols the Ln(|*T*|) and Ψ profiles along the *y* axis corresponding to a film with L = 25 μm buried at depths b = 0.7 (black symbols) and 1.1 mm (red symbols). Measurements have been performed with f = 0.6 Hz, $d \approx$ 0.65 mm and $a \approx$ 0.50 mm. The continuous lines are the least squares fits to Eq. (5) using four free parameters: P_o, a, b and R_{th}. Note that the fit quality is better for Ln|*T*| than for Ψ since the jump at the crack is much higher for the former. The retrieved couples thermal resistance and depth (R_{th}, b) are (0.9×10^{-3} m^{2}K/W, 0.72 mm) and (1.1×10^{-3} m^{2}K/W, 1.3 mm), which correspond to air thicknesses of 23 and 28 μm respectively. Both air gap thickness and depth are very close to the nominal values of the metallic film. On the other hand, in both fittings the radius of the laser spot is in the range a = 0.48-0.52 mm.

We have performed the same measurements but using an AISI-304 film 12.5 μm thick. The same experimental parameters as before have been used. The experimental data are shown by symbols in Fig. 10b together with the fits to Eq. (5), which are represented by the continuous lines. The retrieved couples thermal resistance and depth (R_{th}, b) are (0.45×10^{-3} m^{2}K/W, 0.69 mm) and (0.52×10^{-3} m^{2}K/W, 1.1 mm), which correspond to air thicknesses of 11.5 and 13.5 μm respectively. Both air gap thickness and depth are very close to the nominal values of the metallic film. As before, in both fittings the radius of the laser spot is in the range a = 0.49-0.53 mm.

5. Conclusions

A Bauman-Oden type discontinuous Galerkin finite elements method has been developed to compute the surface temperature of samples containing arbitrarily narrow cracks of any shape when the sample surface is illuminated by a modulated and focused laser beam. The main contribution of this development is that, unlike classical continuous finite elements methods, it allows surface temperature calculations in the presence of very narrow cracks. Besides, computing time and memory resources are kept down to very reasonable values. The simulations performed on semi-infinite and rectangular vertical cracks indicate that the temperature amplitude and phase profiles along the direction normal to the crack through the center of the exciting spot exhibit jumps at both sides of the crack. The height of these jumps is highly sensitive to the crack parameters (depth, thickness and length). In order to check the ability of the method to retrieve these parameters we took lock-in thermography data on samples containing calibrated semi-infinite narrow cracks of different thicknesses and depths. Least squares fitting of the data yielded values of the crack thickness and depth in good agreement with the nominal values. This powerful method opens the possibility of characterizing narrow cracks of arbitrary shape and size from lock-in thermography data.

Acknowledgments

This work has been supported by the Ministerio de Ciencia e Innovación (MAT2011-23811 and MTM2010-16917), by Gobierno Vasco (IT619-13), by UPV/EHU (UFI 11/55), by Diputación General de Aragón, by CINVESTAV Unidad Mérida and by CONACYT beca mixta.

References

[1] Maldague X *Theory and Practice of Infrared Technology for Nondestructive Testing* 2001 (New York: Wiley)
[2] Breitenstein O and Langenkamp M 2003 *Lock-in Thermography* (Berlin: Springer)
[3] Rantala J, Wu D and Busse G 1996 *Res. Nondest. Eval.* **7** 215-28
[4] Favro L D, Han X, Ouyang Z, Sun G, Sui H and Thomas R L 2000 *Rev. Sci. Instrum.* **71** 2418-21.
[5] Piau J-M, Bendada A, Maldague X and Legoux J-G 2008 *Nondestr. Testing Eval.* **23** 109-20.
[6] Renshaw J, Chen J C, Holland S D and Thompson R B 2011 *NDT&E Int.* **44** 736-9.
[7] Mendioroz A, Castelo A, Celorrio R and Salazar A 2013 *Meas. Sci. Technol.* **24** 065601
[8] Morbidini M, Cawley P, Barden T, Almond D and Duffour Ph 2006 *J. Appl. Phys.* **100** 104905
[9] Weekes B, Cawley P, Almond D and Li T 2010 *AIP Conf. Proc.* **1211** 490-7.
[10] Wang Y Q, Kuo P K, Favro L D and Thomas R L 1990 *Springer Series in Optical Science, Photoacoustic and Photothermal Phenomena II* **62** 24-6.
[11] Bodnar JL, Egée M, Menu C, Besnard R, Le Blanc A, Pigeon M and Sellier J Y 1994 *J. de Physique IV, Colloque C7* **4** C7-591-4.
[12] Gruss C, Lepoutre F and Balageas D 1996 *Prog. Nat. Sci. Suppl. vol.* **6**, 173-6.
[13] Krapez J-C 1999 *Int. J. Therm. Sci.* **38** 769-79.
[14] Li T, Almond D P and Rees D A S 2011 *Meas. Sci. Technol.* **22** 035701
[15] Schlichting J, Ziegler M, Dey A, Maierhofer Ch and Kreutzbruck M 2011 *QIRT Journal* **8** 119-23.
[16] Li T, Almond D P and Rees D A S 2011 *NDT&E Int.* **44** 216-25.
[17] Burrows S E, Dixon S, Pickering S G, Li T and Almond D P 2011 *NDT&E Int.* **44** 589-96.
[18] Schlichting J, Maierhofer Ch and Kreutzbruck M 2012 *NDT&E Int.* **45** 133-40.
[19] Streza M, Fedala Y, Roger J P, Tessier G and Boue C 2013 *Meas. Sci. Technol.* **24** 045602
[20] Johnson C 2009 *Numerical Solution of Partial Differential Equations by the Finite Element Method* (Dover).
[21] Douglas N A, Brezzi F, Cockburn B and Marini L D 2002 *SIAM J. Numer. Anal.* **39** 1749-79.
[22] Logg A, Mardal K A and Wells G N Eds. 2012 *Automated Solution of Differential Equations by the Finite Element Method* (Springer)
[23] Hecht F 2012 *J. Numer. Math.* **20** 251-66.
[24] Carslaw H S and Jaeger J C 1959 *Conduction of Heat in Solids* (Oxford: Oxford University Press) p. 20
[25] Parrot J E and Stukes A D 1975 *Thermal conductivity in Solids* (London: Pion) p. 129

Figure captions

Figure 1. (a) Diagram of an opaque material of arbitrary shape containing a finite crack. Γ_g is the illuminated surface, Γ_C is the crack surface, Γ_0 is the non-illuminated external surface of the material, and Ω is the sample volume. (b) Diagram of the meshed sample showing tetrahedra comforming with the crack.

Figure 2. Scheme of (a) a finite vertical crack (in gray) of arbitrary shape, (b) a semi-infinite vertical crack (in gray) of height *b* and (c) a rectangular vertical crack (in gray) of height *b* and length *c*.

Figure 3. Mesh with 6,491 tetrahedra of a cracked thermally thick prism of AISI-304 with dimensions $10\mu \times 8\mu \times 5\mu$ for a modulation frequency f = 0.6 Hz. A semi-infinite crack with depth b = 1 mm is depicted in red.

Figure 4. Simulation of (a) the natural logarithm of the temperature amplitude and (b) phase along the *y* axis for an AISI-304 sample (D = 4 mm^2/s and K = 15 Wm^{-1}K^{-1}) containing a semi-infinite vertical crack of R_{th} = 10^{-3} m^{2}K/W. The sample is illuminated at d = 1 mm with a Gaussian laser spot of a = 0.75 mm modulated at f = 1 Hz. Several crack depths *b* are studied.

Figure 5. Numerical simulation of the dependence of $\Delta_{|T|}$ and Δ_{Ψ} on the thermal contact resistance R_{th}. Calculations are performed for an AISI-304 sample (D = 4 mm^2/s and K = 15 Wm^{-1}K^{-1}) with d = 1 mm, a = 0.75 mm and f = 1 Hz. Several crack depths *b* are analyzed.

Figure 6. The same as in Fig. 4 for f = 0.1 Hz.

Figure 7. The same as in Fig. 5 for f = 0.1 Hz.

Figure 8. Simulation of (a) the natural logarithm of the temperature amplitude and (b) phase along the *y* axis for an AISI-304 sample containing a rectangular vertical crack of R_{th} = 10^{-3} m^{2}K/W. The sample is illuminated at d = 1 mm with a Gaussian laser spot of a = 0.75 mm modulated at f = 1 Hz. The depth b = 0.5 mm is kept while several lengths *c* are studied.

Figure 9. Diagram of the semi-infinite vertical crack simulated for the experiment: A thin film of thickness *L* is sandwiched between two blocks and is buried at a depth *b* beneath the surface. Blocks and film are made of the same material AISI-304 stainless steel.

Figure 10. Experimental Ln(|*T*|) and Ψ of the surface temperature along the *y* axis for two AISI-304 stainless steel blocks sandwiching a thin film (a) 25 μm and (b) 12.5 μm thick of the same material. The thin film is buried at two different depths b = 0.7 mm (black) and 1.1 mm (red). Measurements have been performed with f = 0.6 Hz, $d \approx$ 0.65 mm and $a \approx$ 0.50 mm. Symbols correspond to experimental data and continuous lines to the fit to Eq. (5).